Defect-Engineered Three-Dimensional Graphene–Nanotube–Palladium Nanostructures with Ultrahigh Capacitance

Vadahanambi Sridhar,[†,⊥] Hyun-Jun Kim,[†,⊥] Jung-Hwan Jung,[†] Changgu Lee,[‡] Sungjin Park,[§] and Il-Kwon Oh[†,*]

[†]Graphene Research Center, KAIST Institute for the NanoCentury, Division of Ocean Systems Engineering, School of Mechanical, Aerospace and Systems Engineering, Korea Advanced Institute of Science and Technology, 335 Gwahak-ro, Yuseong-gu, Daejeon 305-701, Republic of Korea, [‡]SKKU Advanced Institute of Nanoscience and Technology, School of Mechanical Engineering, Sungkyunkwan University, 2066 Seobu-ro, Jangangu, Suwon, 440-746, Republic of Korea, and [§]Department of Chemistry, Inha University, 100 Inha-ro, Nam-gu, Incheon 402-751, Republic of Korea. [⊥]These authors contributed equally to this work.

ABSTRACT The development of three-dimensional carbon-based nanostructures is the next step forward for boosting industrial applications of carbon nanomaterials such as graphenes and carbon nanotubes. Some defects, which have been considered as detrimental factors for maintaining exceptional materials properties of two-dimensional graphene, can be actively used to synthesize three-dimensional graphene-based carbon nanostructures. Here we describe a fast and heretofore unreported defect-engineered method to synthesize three-dimensional carbon nanohybrid structures with strong bonding between graphene nanoplatelets and carbon nanotubes using simple microwave irradiation and an ionic liquid. Our one-pot method utilizes defect-engineered sequential processes: microwave-based defect generation on graphene nanoplatelets, anchoring of palladium nanoparticles on these defects, and subsequent growth of carbon nanotubes by use of an ionic liquid. The unique three-dimensional nanostructures showed an ultrahigh redox capacitance due to high porosity, a high surface-to-volume ratio from the spacer role of vertically standing one-dimensional carbon nanotubes on graphene sheets, and capacitance-like redox response of the palladium nanoparticles. The proposed defect-engineered method could lead to novel routes to synthesizing three-dimensional graphene-based nanostructures with exceptionally high performance in energy storage systems.

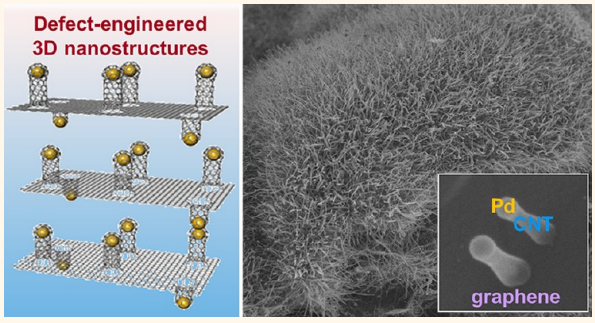

KEYWORDS: graphene · defect engineering · three-dimensional nanostructures · capacitance · microwave · energy storage

Two-dimensional graphene-based nanomaterials[1] have shown important application potential due to their remarkable properties, such as high thermal conductivity,[2] ultrahigh mechanical modulus and strength,[3] wetting transparency,[4] and transparent and stretchable electrodes.[5] Recently, nanoarchitectured, three-dimensional (3D) carbon nanostructures made by connecting two-dimensional (2D) graphene and one-dimensional (1D) carbon nanotubes (CNTs) have attracted great interest, because an ultrahigh surface-to-volume ratio, which is greatly important in energy applications, can be achieved with similar work functions, and reduced agglomeration between nanomaterials can greatly enhance the applicability in industrial fields. The 3D carbon hybrid materials have great advantages for such practical applications as in mechanically compliant films,[6] transparent conductive thin films,[7,8] anodes for lithium ion batteries,[9] supercapacitors,[10] solar cells,[11] reinforcing agents in nanocomposites,[12] and biomedical imaging.[13]

2D and 3D nanohybrids combining graphene and CNTs can be prepared using chemically derived graphene as the starting material, followed by the growth of CNTs *via* thermal CVD,[6,14] by chemically grafting CNTs onto graphene,[15] and by the formation of graphene patches on CNT bucky papers.[16] These hybrids require multistage fabrication processes, and in some cases

* Address correspondence to ikoh@kaist.ac.kr.

Received for review June 30, 2012 and accepted November 1, 2012.

Published online November 01, 2012
10.1021/nn3046133

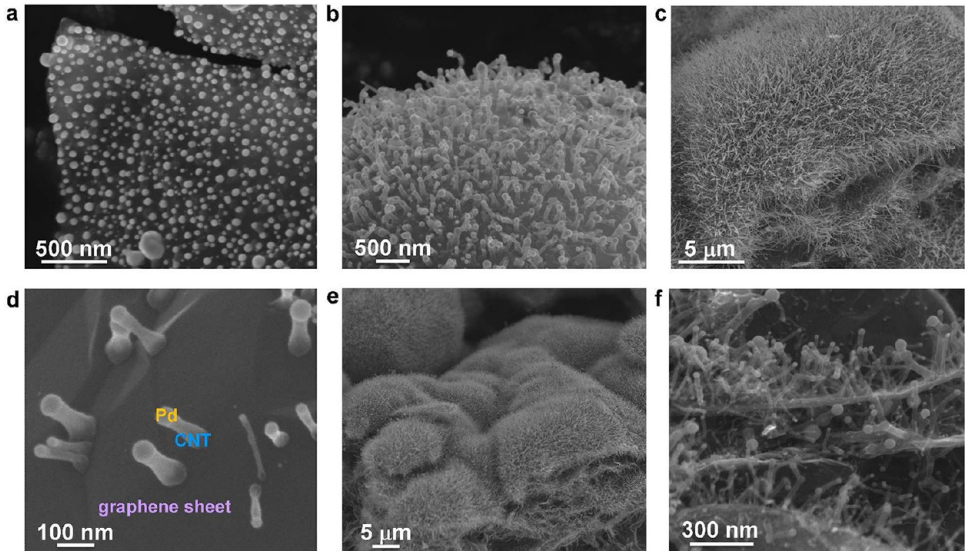

Figure 1. SEM micrographs of 3D carbon nanostructures showing CNTs vertically attached to graphene nanoplatelets: (a) palladium nanoparticles initially anchored on a graphene, (b) vertically standing CNTs grown on graphene by palladium nanoparticles, (c) CNT forest extensively grown on graphene surfaces after lengthy microwave radiation, (d) direct bonding between CNTs and graphene, (e) mass production of 3D G–CNT–Pd nanostructures, and (f) terraced structure of multilevel G–CNT–Pd hybrids.

they suffer from property limitations due to weak binding between the CNTs and graphene. However, making strong bonding between carbon nanostructures is a great challenge in recent nanotechnology.

To date, atomic scale defects in the nanofabrication process have been considered to be removed for preserving intrinsically exceptional mechanical, electrical, and thermal properties of carbon nanomaterials. Especially, high-quality and defect-free graphene syntheses[17,18] including a mechanical exfoliation method, chemical methods, unzipping methods, chemical vapor deposition, and epitaxial growth methods have been developed for careful defect control of 2D graphene sheets. However, the atomic scale defects on graphene can be actively engineered to synthesize 3D carbon nanostructures with designed multifunctional properties. When a crystal of a carbon nanostructure grows, different imperfections, which can be classified as either point defects, dislocations, or plane defects, can play an important role in initiating the growth as nucleation sites of catalytic metal nanoparticles. Intentionally designed defects can be introduced to construct hierarchical 3D carbon nanostructures with strong bonding between graphene and CNTs.

Here, we report a unique defect-engineered microwave method to produce a 3D carbon nanostructure of graphene–carbon nanotube–palladium (G–CNT–Pd) that consists of carbon nanotubes vertically standing on graphene sheets with direct covalent bonding and palladium nanoparticles attached at the top of the carbon nanotubes. The resulting 3D G–CNT–Pd nanostructures show an ultrahigh redox capacitance due to high porosity, a high surface-to-volume ratio, and capacitance-like redox response of the palladium nanoparticles.

RESULTS AND DISCUSSION

Figure 1 shows SEM micrographs of 3D carbon nanostructures synthesized by the present microwave method. At the initial stage of microwave irradiation, palladium nanoparticles are anchored on a graphene sheet as shown in Figure 1a. After further radiation, as shown in Figure 1b, the palladium nanoparticles induce vertical growth of carbon nanotubes on graphene sheets. Figure 1c shows that the carbon nanotubes are extensively grown on graphene surfaces after sustained radiation, resulting in a CNT forest on the graphene ground. Densely grown carbon nanotubes can play an important role in increasing the surface-to-volume ratio of the 3D carbon nanostructures. Here a question about the bonding between carbon nanotubes and graphene may arise. Figure 1d shows direct bonding between carbon nanotubes and graphene due to the defect-based growth mechanism. Also, it is possible to produce large amounts of the 3D G–CNT–Pd nanostructure through the one-pot microwave method with large quantities of graphene platelets, as shown in Figure 1e. From the expandable few-layered graphene sheets, a terraced structure of multilevel G–CNT–Pd hybrids can be obtained, as shown in Figure 1f. The vertically aligned CNTs between graphene sheets will not only improve the surface area of graphene materials but also act as spacers to facilitate a diffusion path for the rapid transport of electrolyte ions and thermal exchange in 3D nanostructures.

High-resolution SEM micrographs depict the uniqueness of the nanohybrid structure with carbon

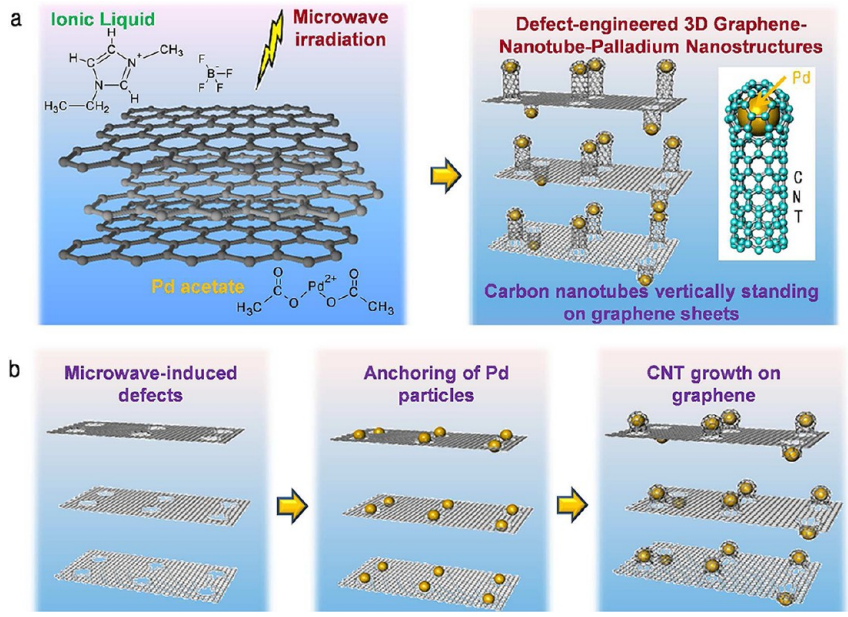

Figure 2. One-pot microwave synthesis of three-dimensional carbon hybrid nanostructures showing vertically grown carbon nanotubes on graphene sheets: (a) scheme and (b) mechanism.

nanotubes firmly anchored to the graphene surface and palladium particles attached at the top of the carbon nanotubes. This morphology is unique and differs from those described in earlier reports[6,14] of CVD-grown CNTs on metal particles deposited on graphene surfaces. One disadvantage of growing CNTs on a metal–graphene substrate by CVD is that the CNTs are anchored to the metal catalyst particles rather than to the graphene sheet itself, because the CNTs are grown by a "base growth mechanism". Therefore, if catalyst particles delaminate from the graphene surface, the CNTs also drop off. However, in the present case, the catalyst particles are located on the tips of CNTs, indicating a "tip growth mechanism". Once the CNTs are directly formed on a graphene nanosheet with covalent bonding, there is no direct interaction between the metal nanoparticles and the graphene surface. Therefore, even when the palladium particle delaminates and falls off the nanotube, the CNT remains well anchored to the graphene substrate.

The mechanism of CNT growth on graphene sheets can be explained as follows: first, impregnation and partial exfoliation of graphene platelets in ionic liquids take place in the mixture of few-layered graphene platelets, palladium acetate, and EMIM-BF_4 due to weak van der Waal's and $\pi-\pi$ interactions.[19] The Pd cation and acetate anion of the palladium salt will be coordinately dissolved by the BF_4^- anion and the larger imidazolium cation of the ionic liquid, respectively. Consequently, the Pd^+ cation can be reduced due to the reducing characteristic of the ionic liquid, and the palladium nanoparticles are distributed on the graphene sheets.[20,21] Second, when the mixture is subjected to microwave irradiation, the graphene platelet is fully exfoliated to form graphene nanosheets with atomic defects, which may be caused by either the catalytic activity of the ionic liquid or microwave radiation. These defects on the graphene surface act as nucleation and anchoring sites for imidazolium-shelled palladium nanoparticles (Figure S2a in the Supporting Information). The morphology of this intermediate phase will hence resemble imidazolium-shelled palladium nanoparticles very finely dispersed on graphene sheets (Figure S2b in the Supporting Information). Finally, with further microwave irradiation, the imidazolium component of the ionic liquid decomposes to produce carbonaceous gases that serve as carbon sources for the CNT growth. These gases are captured by the palladium nanoparticles to form carbon-coated palladium core–shell nanoparticles, which subsequently transform into nanotubes *via* a mechanism analogous to the classic "tip-growth" dissolution–extrusion process. Carbon diffuses on the exposed palladium particles, forming multiwalled "core-shelled' carbon–palladium nanoclusters and precipitate at the tail end of the "teardrop"-shaped particles, forming tubular graphitic cones. This creation of fresh cones proceeds until the shape of the palladium changes from the unstable "teardrop" to the more stable crystalline palladium. The total synthesis and mechanism are schematically illustrated in Figure 2. As the first unexpected SEM observation of 3D nanostructures, the vertical growth of carbon nanotubes predominantly at the edges and rarely on the surfaces of graphene nanosheets is shown in Figure S1. This can be attributed to the defect-based growth mechanism describing the anchoring sites of carbon nanotubes, which are

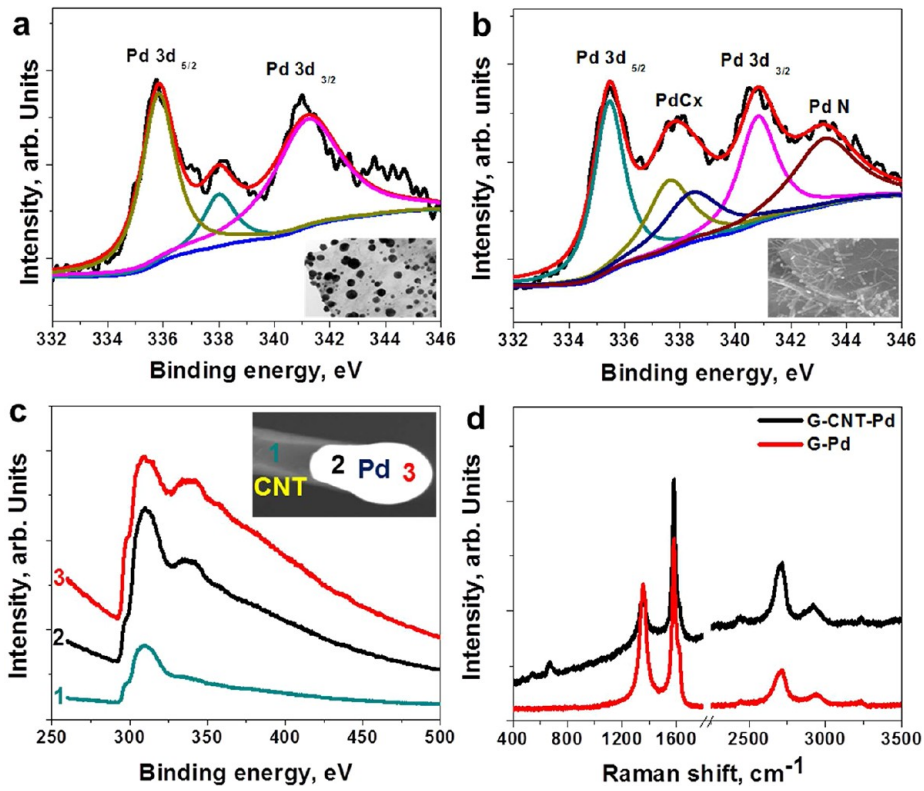

Figure 3. Deconvoluted XPS spectra of (a) G−Pd without CNT growth and (b) G−CNT−Pd; (c) EELS spectra of encapsulated palladium at various positions; (d) Raman spectra changes in graphene-based nanohybrids with and without CNT growth.

predominantly grown at the edges rather than on the surface of graphene sheets.

In order to further prove that the carbon source for the CNT growth is from the ionic liquid, we carried out two separate tests involving a first reactant mixture of palladium and ionic liquid (EMIM BF_4) alone without graphene and a second reactant mixture of palladium and graphene alone without ionic liquid by using urea as a reducing agent[22] and subjecting these two reactant mixtures to microwave irradiation. The morphologies of the products obtained from these two different tests are shown in Figure S3 of the Supporting Information. In the first case, extensive formation of carbon nanotubes can be observed. In the second case, extensive cutting of the graphene sheets due to the mobility of palladium nanoparticles occurred, and CNT growth was not seen, as previously reported.[23] These two results conclusively confirm that the carbonaceous byproducts that evolve due to the microwave-induced decomposition of the imidazolium moiety of the ionic liquid are the carbon source for the growth of carbon nanotubes on the graphene surfaces.

Evidence of chemical transformations in palladium particles can be observed in the deconvoluted XPS spectra for both G−Pd without carbon nanotube growth[18] and G−CNT−Pd, as plotted in Figure 3a and b, respectively. Deconvoluted XPS spectra of the G−Pd nanosheet plotted in Figure 3a show two major peaks,[24] at 335.4 and 340.8 eV, in the Pd $3d_{3/2}$ and Pd $3d_{5/2}$ regions, respectively, with spin−orbit splitting of the $3d_{5/2}$ and $3d_{3/2}$ states at 5.3 eV, indicating the existence of more than one chemical state of palladium nanoparticles. The dominant Pd $3d_{5/2}$ peak with a binding energy of 335.4 eV is characteristic of so-called "electron-deficient" Pd species, such as Pd^{+} or $Pd^{\delta+}$ ($0 < \delta < 1$). In case of the G−CNT−Pd 3D nanostructure, besides these two peaks at 335.4 and 340.8 eV, two additional peaks at 337.8 and 343.2 eV, indicating the formation of PdCx[25] and PdN[26] moieties, respectively, are observed, as shown in Figure 3b. The formation of PdCx indicates chemisorption of carbon onto the palladium surface and the formation of CNTs by the well-known "tip-growth" dissolution−extrusion model as discussed earlier. The presence of the PdN peak is interesting and can explain the formation of bamboo-shaped carbon nanotubes.[27]

In order to study the chemical changes in the vicinity of palladium nanoparticles, we used EELS spectra. The inset in Figure 3c shows annular dark-field (ADF) images obtained during the EELS point spectra acquisition. The EELS spectra showing the chemical composition at three different points are plotted in Figure 3c. The EELS spectra obtained on the walls of the nanotubes show pure carbon peaks, whereas the spectra at the head of the palladium nanoparticle show a palladium peak in addition to the carbon peaks. These results confirm that the palladium particle is encapsulated inside the carbon nanotube.

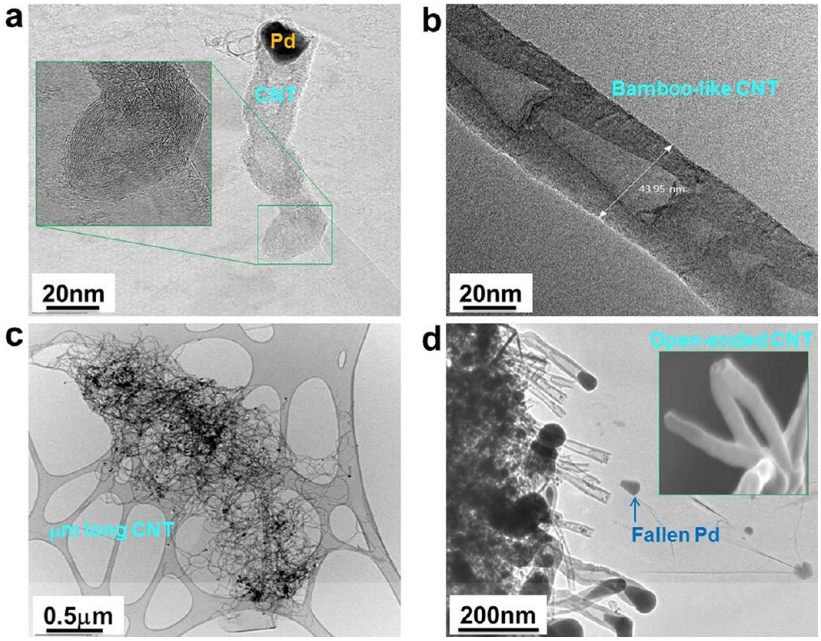

Figure 4. TEM micrographs of vertically standing carbon nanotubes on graphene sheets: (a) anchored carbon nanotube, (b) bamboo-like carbon nanotube, (c) a bunch of micrometer-long carbon nanotubes, and (d) detached palladium nanoparticles and open-ended carbon nanotubes (SEM).

Raman spectroscopy is a powerful tool to investigate structural changes in carbonaceous materials, and the spectra of 2D G−Pd and 3D G−CNT−Pd nanostructures are plotted in Figure 3d. The Raman spectra of carbonaceous materials are characterized by three main features: in the case of graphene, the G mode due to the emission of zone-center optical phonons (usually observed at ∼1575 cm^{-1}), a disorder-induced D mode (∼1350 cm^{-1}), and a symmetry-allowed 2D overtone (∼2700 cm^{-1}). The spectra of both samples show G-bands at 1583 and 1584 cm^{-1}, respectively, and a D-band at 1358 and 1359 cm^{-1}. Although the shifts in the band locations are not substantial, the shapes of the peaks provide valuable information regarding the defects. The D-band in the 2D G−Pd sheet at 1358 cm^{-1} is significantly narrower and thinner than that in the 3D G−CNT−Pd nanostructure. The D-band in graphene at 1357 cm^{-1} and the D′-shoulder at 1620 cm^{-1} are attributed to structural disorder at defect sites and finite size effects, respectively. In the case of the 3D G−CNT−Pd nanostructure, this D′-band at 1620 cm^{-1} is considerably weaker, indicating "partial healing" of defects by the grown carbon nanotubes. The intensity ratio of the D-band to the G-band is also used as a measure of the quality of the graphitic structures. In the case of the 2D G−Pd sheet, the D/G intensity ratio is 0.74 due to the presence of Pd nanoparticles on the graphene sheets, which induce structural disorder and defects within the graphene sheets. However, this D/G intensity ratio reduces to 0.51 in 3D G−CNT−Pd nanohybrids, confirming that the growth of CNTs can facilitate healing of the defects of graphene substrates and a lot of CNTs can increase relatively G-band peaks. Based on entropy considerations, the palladium particles should travel along the defect sites, since the energy of mobility through defects is less when compared to that through defect-free sites.[28] More information confirming the growth of CNTs can be obtained from the second-order Raman spectra, the main lines of which are at 2450, 2705 cm^{-1} (G′), 2945 cm^{-1} (D+G), 3176 cm^{-1} (2G), and 3244 cm^{-1} (2D′). After CNT growth, considerable increases in the intensities of all these peaks can be observed.

High-resolution TEM (HR-TEM) images of an individual nanotube show the anchoring region of the CNT on the graphene surface (Figure 4a and its inset). The root area of the carbon nanotube bonded with the graphene sheet does not include palladium components, which should appear in back in the HR-TEM image. This state of anchoring indicates strong adhesive bonding between two nanostructures, resulting in enhanced durability of the hybrid nanostructures. The 3D G−CNT−Pd nanostructures with covalent bonding endured ultrasonication for more than 30 min without detachments. The nanotubes have bamboo structures with a thickness of around 20−50 nm, as shown in Figure 4b. Also, bunches of micrometer-long agglomerated CNTs on graphene surfaces can be realized by controlling the microwave radiation time, as shown in Figure 4c. One interesting observation is the formation of open-ended carbon nanotubes due to detachment of the palladium nanoparticles, as shown in Figure 4d.

A detached catalytic palladium nanoparticle induces regrowth of another CNT at a different location on the graphene, as shown in the Supporting Information.

This indicates that the shape of the catalyst plays a critical role in the catalytic activity of palladium in the process of CNT growth. If the shape of palladium is retained as a "teardrop" (Figure S4a), then it is catalytically active[29] and can regrow fresh CNTs after falling away. If the shape of palladium is spherical, then it will be catalytically inactive and stable, as shown in Figure S4b of the Supporting Information.

The unique structure of the 3D G−CNT−Pd nanostructure where CNTs are anchored on graphene and palladium particles are enclosed in the carbon nanotubes offers distinct advantages in energy storage systems such as supercapacitors and lithium ion batteries. Supercapacitors offer a safer, longer-cycle-life, and maintenance-free alternative power source when compared to lithium ion or lead acid batteries. The energy storage mechanism of supercapacitors can be broadly divided into two categories: electric double layer capacitance (EDLC) and pseudocapacitance. Double-layer capacitors are composed of all-carbon electrodes, and the capacitance arises from the charges accumulated at the interfaces between the electrode and electrolyte. Activated carbons or porous carbons have been the most widely used materials to date, but recently new allotropes of carbon such as carbon nanotubes and graphene have been investigated. One of the main drawbacks of using graphene in supercapacitors is that the graphene sheets have a high tendency to restack, leaving behind intergraphene pore sizes that are not sufficient for accessibility to the electrolyte and the formation of EDLC charges. In order to overcome this problem, some researchers have used a combination of graphene and CNTs for supercapacitors.[10,21] An alternative to EDLC is pseudocapacitors, which usually consist of hybrids of carbon nanostructures such as graphene or carbon nanotubes with conducting polymers such as polyaniline or metal oxides, especially ruthenium oxide, which has the highest capacitance value thus far. The main drawback of pseudocapacitors, however, is a progressive decrease in charge storage during the multiple charge and discharge cycles due to irreversible Faradic red-ox reactions occurring primarily at the metal oxides. The specific surface area of three nanomaterials was measured with the N_2 adsorption Brunauer−Emmett−Teller (BET) method. The measured BET values of rGO, G−Pd, and G−CNT−Pd are 517.12, 293.07, and 397.20 m^2/g, respectively. Because the BET value is divided by total mass, the carbon−palladium hybrids have relatively high values. The 2D G−Pd hybrid does not have high BET values because of the high weight of palladium particles, while 3D G−CNT−Pd nanostructures show relatively high BET values due to the large surface area of bamboo-shaped carbon nanotubes.

The cyclic voltammetry responses of reduced graphene oxide (rGO), 2D G−Pd, and 3D G−CNT−Pd nanostructures were tested in two different potential ranges of [0 V, +0.6 V] and [−1.0 V, +0.6 V] at a scan rate of 100 mV/s, as shown in Figure 5a and c. In Figure 5a, the 3D G−CNT−Pd nanostructures synthesized in the present study show a maximum current density of 48.2 A/g compared to 8.4 A/g in 2D G−Pd nanostructures. This exceptionally high current density in 3D nanostructures can be attributed to the unique 3D hierarchical carbon nanostructures that provide low diffusion resistance to charge, easy electrolyte penetration, and high electro-active areas. An obvious increase of current density is observed with increasing scan rates, indicating good rate capability of our 3D G−CNT−Pd composite electrodes. Under the positive potential range of [0 V, +0.6 V], the measured specific capacitances of reduced graphene oxide, 2D G−Pd, and 3D G−CNT−Pd nanostructures at various scan rates (10−100 mV/s) are shown in Figure 5b. At the lowest scan rate of 10 mV/s and with the potential window of [0 V, +0.6 V], 3D G−CNT−Pd nanostructures show an outstanding specific capacitance value of 597 F/g, which progressively decreases to 345 F/g at a scan rate of 100 mV/s. The specific capacitance of 2D G−Pd and 3D G−CNT−Pd nanostructures under the potential window of [−1.0 V, +0.6 V] increases more than 3 times, although that of rGO remains almost the same, in comparison with cyclic voltammetry responses of the positive potential window. This clearly demonstrates the effect of palladium nanoparticles on the pseudocapacitance as well as electric double-layer capacitance. The vertically aligned CNTs on the graphene surface will not only improve the surface area of the graphene materials but also act as spacers[30−32] to prevent graphene sheets from restacking and to facilitate diffusion paths for the rapid transport of electrolyte ions within the 3D G−CNT−Pd electrode, resulting in outstanding improvement of the electrochemical properties of the 3D G−CNT−Pd nanostructures.

The high values of specific capacitance at all measured scan rates imply synergetic utilization of both pseudocapacitance due to the presence of palladium nanoparticles and electric double-layer capacitance due to the unique arrangement of two different carbon allotropes, 1D carbon nanotubes vertically standing on 2D graphene sheets. The cyclic voltammetry responses in the potential ranges of [−1.0 V, +0.6 V] at a scan rate of 100 mV/s are shown in Figure 5c. As shown in Figure 5c, the 3D G−CNT−Pd nanostructures synthesized in the present study show a maximum current density of 74.8 A/g compared to 23.02 A/g in 2D G−Pd nanostructures. The interesting observation is the reversible anodic peak occurring at −0.275 V, which corresponds to the conversion reaction of palladium particles in an alkaline KOH electrolyte solution, indicating pseudocapacitance characteristics of the 3D G−CNT−Pd nanostructures. Under the potential range of [−1.0 V, +0.6 V], the measured specific capacitances of reduced graphene oxide, 2D G−Pd, and 3D

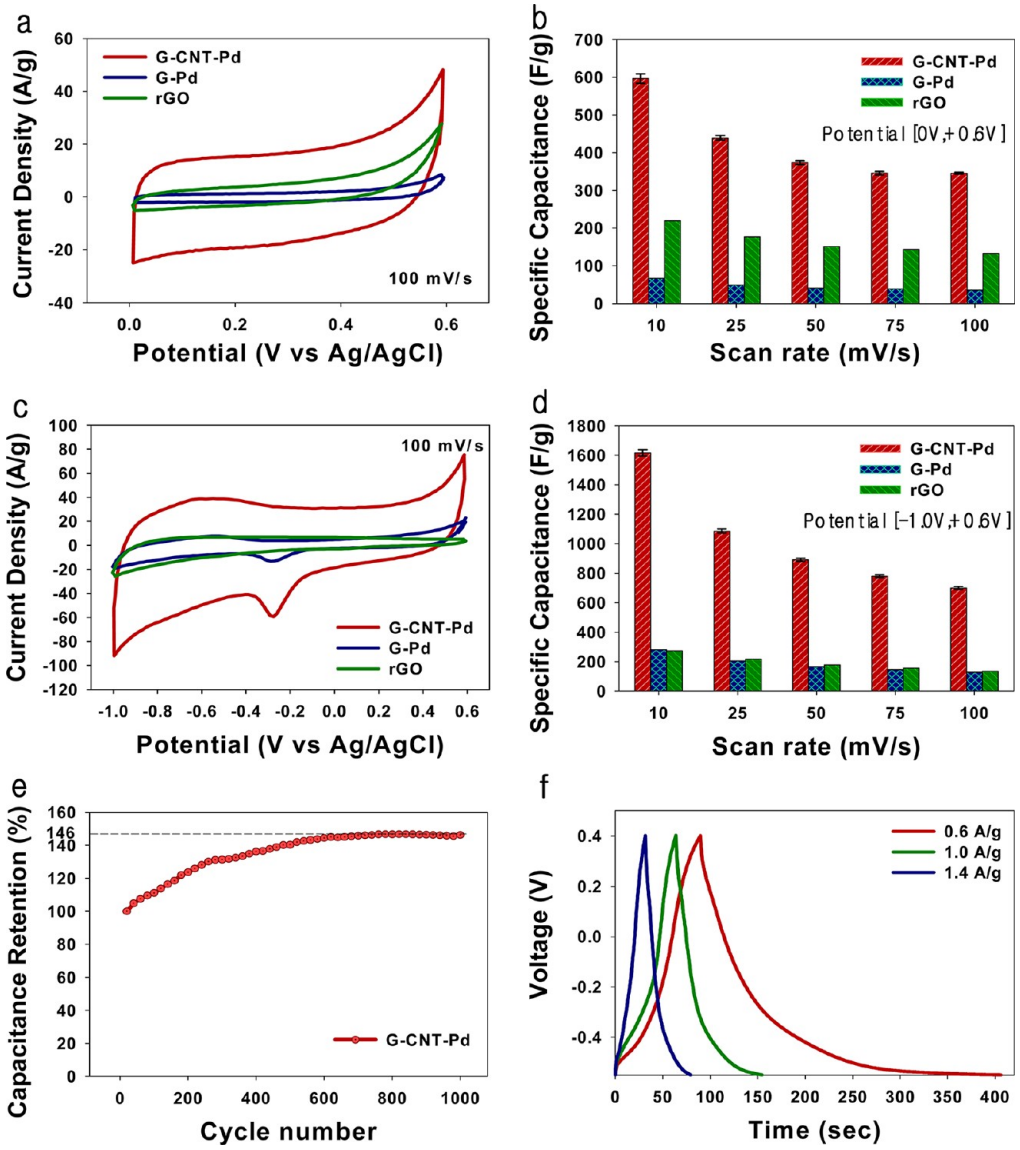

Figure 5. Capacitance tests: (a) current−voltage responses of G−CNT−Pd, G−Pd, and reduced graphene oxide under a potential window of [0 V, +0.6 V], (b) specific capacitances according to the scan rates under a potential window of [0 V, +0.6 V], (c) current−voltage responses of G−CNT−Pd, G−Pd, and reduced graphene oxide under a potential window of [−1.0 V, +0.6 V], (d) specific capacitances according to the scan rates under a potential window of [−1.0 V, +0.6 V], (e) capacitance retention history for 1000 cycles, and (f) charge−discharge responses of G−CNT−Pd nanostructures at different current densities.

G−CNT−Pd nanostructures at various scan rates (10−100 mV/s) are shown in Figure 5d. The G−CNT−Pd nanostructures show an outstanding specific capacitance value of 1615 F/g at the lowest scan rate of 10 mV/s, and the specific capacitance progressively decreases to 700 F/g at a scan rate of 100 mV/s.

Regarding electrochemical reactions of palladium in the KOH solution, some previous studies[33−36] reveal redox states of palladium itself. It has been widely accepted that OH^- ions are first chemisorbed in the initial stage of the oxide formation, and then they are transformed into higher valence oxides at higher potentials[34,35] as described by

$$Pd + OH^- \leftrightarrow PdOH_{ads} + e^- \quad (1)$$

$$PdOH_{ads} + OH^- \leftrightarrow PdO + H_2O + e^- \quad (2)$$

The mild oxidation peaks, which correspond to different electrochemical processes occurring on the surface of the palladium particles, are observed during the positive-going sweep in Figure 5c. The peak around −0.6 V can be attributed to the formation of the palladium(II) oxide layer on the surface of the catalyst. Corresponding to the oxidation process, the reduction of the palladium oxide during the cathodic sweep can be described as

$$PdO + H_2O + 2e^- \leftrightarrow Pd + 2OH^- \quad (3)$$

The CV response of 3D G−CNT−Pd nanostructures as shown in Figure 5c has very similar oxidation and

reduction peak positions in comparison with redox states of palladium itself, as described in ref 33. The well-defined reduction peak of palladium lies in the potential range from −0.15 to −0.45 V, mainly around −0.275 V. The redox states of palladium particles contribute to the pseudocapacitance of the 3D G−CNT−Pd nanostructures in the potential window of [−1.0 V, +0.6 V].

The electrochemical durability of the G−CNT−Pd nanomaterial at a scan rate of 100 mV/s for 1000 cycles is shown in Figure 5e. A capacitance increase of about 46% relative to the initial capacitance after 600 cycles has been observed, with the capacitance stabilizing even until 1000 cycles. This excellent electrochemical stability and retention of the 3D G−CNT−Pd electrode material is crucial for the practical application of supercapacitors. Also, charge−discharge diagrams of 3D G−CNT−Pd nanostructures are shown in Figure 5f with different current densities. High surface-to-volume ratio, removal of restacking of 2D nanostructures, and nitrogen-doped bamboo-shaped CNTs in the 3D G−CNT−Pd nanostructures play a synergistic role in ultrahigh capacitance as well as pseudocapacitance of palladium nanoparticles.

CONCLUSION

We have grown CNTs on graphene nanosheets to form unique 3D carbon nanostructures. This has been achieved by a simple defect-engineered technique using an ionic liquid, a palladium catalyst, and microwave radiation. Despite its simplicity, the proposed method is an effective way to overcome the cost and operational limitations of thermal CVD and yields nanohybrids of CNTs firmly anchored onto graphene nanosheets, a major challenge in today's graphene research. The unique structure endows high-rate transportation of electrolyte ions and electrons throughout the electrode matrix and comprehensive utilization of pseudo and double-layer capacitance, resulting in excellent electrochemical performances. The capacitance of 3D G−CNT−Pd exhibits an exceptionally high value at a scan rate of 10 mV/s even in a weak electrolyte solution of 1 M KOH. After 600 cycles, a capacitance increase of 46% relative to the initial capacitance is observed, indicating excellent electrochemical stability of the electrode. We believe that this unique and versatile method for the synthesis of 3D carbon nanostructures, whose functionality can be tailored by changing the catalyst with cobalt, nickel, and other metals, will open a new era for practical applications such as supercapacitors, lithium ion batteries, media for hydrogen storage, catalysts for fuel cells, sensors, and actuators, materials for energy storage, and biomedical devices.

METHODS

This one-pot microwave method for the 3D carbon nanostructure, which is suitable for upscale, is simple and utilizes three ingredients: expandable graphene platelets (Samjung C&G), a palladium(II) acetate catalytic precursor (98%, Sigma-Aldrich), and an ionic liquid (EMIM BF_4, Merck). These ingredients were mixed with the same weight of 0.5 g and ultrasonicated for 30 min. Subsequently, the mixture was subjected to microwave irradiation at 700 W for about 10 min to yield a fluffy powder of carbon nanohybrid. This synthesis can be achieved even with palladium nanoparticles and can be used to generate nanometer-sized tubular carbon clusters firmly bonded to graphene surfaces and edges.

Conflict of Interest: The authors declare no competing financial interest.

Acknowledgment. This work was supported by a National Research Foundation of Korea Grant funded by the Korean Government (No. R0A-2008-000-20012-0 and 2012R1A2A2A0104754). It was also supported by a grant from the Fundamental R&D Programs for Core Technology of Materials funded by the Ministry of Knowledge Economy, Republic of Korea [K0006028]. This research was supported by KAIST Institute for the NanoCentury.

Supporting Information Available: The supporting file shows indirect evidence of defect-engineered 3D carbon nanostructures where vertically standing carbon nanotubes are densely grown along graphene edges with defects and relatively sparse carbon nanotubes are grown on the graphene surface. SEM and TEM images of imidazolium-shelled palladium nanoparticles, micrometer-long carbon nanotubes grown with palladium nanoparticles, and shapes of palladium nanoparticles inducing carbon nanotubes are provided. This material is available free of charge *via* the Internet at http://pubs.acs.org.

REFERENCES AND NOTES

1. Geim, A. K.; Novoselov, K. S. The Rise of Graphene. *Nat. Mater.* **2007**, *6*, 183–191.
2. Chen, S. S.; Wu, Q. Z.; Mishra, C.; Kang, J. Y.; Zhang, H. J.; Cho, K. J.; Cai, W. W.; Balandin, A. A.; Ruoff, R. S. Thermal Conductivity of Isotopically Modified Graphene. *Nat. Mater.* **2012**, *11*, 203–207.
3. Lee, C.; Wei, X. D.; Kysar, J. W.; Hone, J. Measurement of the Elastic Properties and Intrinsic Strength of Monolayer Graphene. *Science* **2008**, *321*, 385–388.
4. Rafiee, J.; Mi, X.; Gullapalli, H.; Thomas, A. V.; Yavari, F.; Shi, Y. F.; Ajayan, P. M.; Koratkar, N. A. Wetting Transparency of Graphene. *Nat. Mater.* **2012**, *11*, 217–222.
5. Kim, K. S.; Zhao, Y.; Jang, H.; Lee, S. Y.; Kim, J. M.; Kim, K. S.; Ahn, J. H.; Kim, P.; Choi, J. Y.; Hong, B. H. Large-Scale Pattern Growth of Graphene Films for Stretchable Transparent Electrodes. *Nature* **2009**, *457*, 706–710.
6. Lee, D. H.; Kim, J. E.; Han, T. H.; Hwang, J. W.; Jeon, S.; Choi, S. Y.; Hong, S. H.; Lee, W. J.; Ruoff, R. S.; Kim, S. O. Versatile Carbon Hybrid Films Composed of Vertical Carbon Nanotubes Grown on Mechanically Compliant Graphene Films. *Adv. Mater.* **2010**, *22*, 1247–1252.
7. Kim, Y. K.; Min, D. H. Durable Large-Area Thin Films of Graphene/Carbon Nanotube Double Layers as a Transparent Electrode. *Langmuir* **2009**, *25*, 11302–11306.
8. Hong, T.-K.; Lee, D. W.; Choi, H. J.; Shin, H. S.; Kim, B.-S. Transparent, Flexible Conducting Hybrid Multilayer Thin Films of Multiwalled Carbon Nanotubes with Graphene Nanosheets. *ACS Nano* **2010**, *4*, 3861–3868.
9. Zhu, X. J.; Zhu, Y. W.; Murali, S.; Stollers, M. D.; Ruoff, R. S. Nanostructured Reduced Graphene Oxide/Fe_2O_3 Composite As a High-Performance Anode Material for Lithium Ion Batteries. *ACS Nano* **2011**, *5*, 3333–3338.
10. Kim, Y. S.; Kumar, K.; Fisher, F. T.; Yang, E. H. Out-of-Plane Growth of CNTs on Graphene for Supercapacitor Applications. *Nanotechnology* **2012**, *23*, 015301–1−7.

11. Yen, M. Y.; Hsiao, M. C.; Liao, S. H.; Liu, P. I.; Tsai, H. M.; Ma, C. C. M.; Pu, N. W.; Ger, M. D. Preparation of Graphene/Multi-Walled Carbon Nanotube Hybrid and Its Use as Photoanodes of Dye-Sensitized Solar Cells. *Carbon* **2011**, *49*, 3597–3606.
12. Vickery, J. L.; Patil, A. J.; Mann, S. Fabrication of Graphene-Polymer Nanocomposites with Higher-Order Three-Dimensional Architectures. *Adv. Mater.* **2009**, *21*, 2180–2184.
13. Kim, Y. K.; Na, H. K.; Kwack, S. J.; Ryoo, S. R.; Lee, Y.; Hong, S.; Hong, S.; Jeong, Y.; Min, D. H. Synergistic Effect of Graphene Oxide/MWCNT Films in Laser Desorption/Ionization Mass Spectrometry of Small Molecules and Tissue Imaging. *ACS Nano* **2011**, *5*, 4550–4561.
14. Paul, R. K.; Ghazinejad, M.; Penchev, M.; Lin, J. A.; Ozkan, M.; Ozkan, C. S. Synthesis of a Pillared Graphene Nanostructure: A Counterpart of Three-Dimensional Carbon Architectures. *Small* **2010**, *6*, 2309–2313.
15. Tung, V. C.; Chen, L. M.; Allen, M. J.; Wassei, J. K.; Nelson, K.; Kaner, R. B.; Yang, Y. Low-Temperature Solution Processing of Graphene-Carbon Nanotube Hybrid Materials for High-Performance Transparent Conductors. *Nano Lett.* **2009**, *9*, 1949–1955.
16. Li, C. Y.; Li, Z.; Zhu, H. W.; Wang, K. L.; Wei, J. Q.; Li, X. A.; Sun, P. Z.; Zhang, H.; Wu, D. H. Graphene Nano-"patches" on a Carbon Nanotube Network for Highly Transparent/Conductive Thin Film Applications. *J. Phys. Chem. C* **2010**, *114*, 14008–14012.
17. Li, X. S.; Cai, W. W.; An, J. H.; Kim, S.; Nah, J.; Yang, D. X.; Piner, R.; Velamakanni, A.; Jung, I.; Tutuc, E.; *et al*. Large-Area Synthesis of High-Quality and Uniform Graphene Films on Copper Foils. *Science* **2009**, *324*, 1312–1314.
18. Reddy, C. D.; Ramasubramaniam, A.; Shenoy, V. B.; Zhang, Y. W. Edge Elastic Properties of Defect-Free Single-Layer Graphene Sheets. *Appl. Phys. Lett.* **2009**, *94*, 101904-1–3.
19. Scheuermann, G. M.; Rumi, L.; Steurer, P.; Bannwarth, W.; Mulhaupt, R. Palladium Nanoparticles on Graphite Oxide and Its Functionalized Graphene Derivatives as Highly Active Catalysts for the Suzuki-Miyaura Coupling Reaction. *J. Am. Chem. Soc.* **2009**, *131*, 8262–8270.
20. Zhang, L. L.; Xiong, Z. G.; Zhao, X. S. Pillaring Chemically Exfoliated Graphene Oxide with Carbon Nanotubes for Photocatalytic Degradation of Dyes under Visible Light Irradiation. *ACS Nano* **2010**, *4*, 7030–7036.
21. Fan, Z. J.; Yan, J.; Zhi, L. J.; Zhang, Q.; Wei, T.; Feng, J.; Zhang, M. L.; Qian, W. Z.; Wei, F. A Three-Dimensional Carbon Nanotube/Graphene Sandwich and Its Application as Electrode in Supercapacitors. *Adv. Mater.* **2010**, *22*, 3723–3728.
22. Wang, X. Q.; Fulvio, P. F.; Baker, G. A.; Veith, G. M.; Unocic, R. R.; Mahurin, S. M.; Chi, M. F.; Dai, S. Direct Exfoliation of Natural Graphite into Micrometre Size Few Layers Graphene Sheets Using Ionic Liquids. *Chem. Commun.* **2010**, *46*, 4487–4489.
23. Campos, L. C.; Manfrinato, V. R.; Sanchez-Yamagishi, J. D.; Kong, J.; Jarillo-Herrero, P. Anisotropic Etching and Nanoribbon Formation in Single-Layer Graphene. *Nano Lett.* **2009**, *9*, 2600–2604.
24. Peuckert, M. XPS Study on Surface and Bulk Palladium Oxide, Its Thermal-Stability, and a Comparison with Other Noble-Metal Oxides. *J. Phys. Chem.* **1985**, *89*, 2481–2486.
25. Teschner, D.; Borsodi, J.; Wootsch, A.; Revay, Z.; Havecker, M.; Knop-Gericke, A.; Jackson, S. D.; Schlogl, R. The Roles of Subsurface Carbon and Hydrogen in Palladium-Catalyzed Alkyne Hydrogenation. *Science* **2008**, *320*, 86–89.
26. Parambhath, V. B.; Nagar, R.; Ramaprabhu, S. Effect of Nitrogen Doping on Hydrogen Storage Capacity of Palladium Decorated Graphene. *Langmuir* **2012**, *28*, 7826–7833.
27. Gong, K. P.; Du, F.; Xia, Z. H.; Durstock, M.; Dai, L. M. Nitrogen-Doped Carbon Nanotube Arrays with High Electrocatalytic Activity for Oxygen Reduction. *Science* **2009**, *323*, 760–764.
28. Sundaram, R. S.; Gomez-Navarro, C.; Balasubramanian, K.; Burghard, M.; Kern, K. Electrochemical Modification of Graphene. *Adv. Mater.* **2008**, *20*, 3050–3053.
29. Hofmann, S.; Sharma, R.; Ducati, C.; Du, G.; Mattevi, C.; Cepek, C.; Cantoro, M.; Pisana, S.; Parvez, A.; Cervantes-Sodi, F.; *et al*. In Situ Observations of Catalyst Dynamics During Surface-Bound Carbon Nanotube Nucleation. *Nano Lett.* **2007**, *7*, 602–608.
30. Wang, Y.; Wu, Y.; Huang, Y.; Zhang, F.; Yang, X.; Ma, Y.; Chen, Y. Preventing Graphene Sheets from Restacking for High-Capacitance Performance. *J. Phys. Chem. C* **2011**, *115*, 23192–23197.
31. Salgado, S.; Pu, L.; Maheshwari, V. Targeting Chemical Morphology of Graphene Oxide for Self-Assembly and Subsequent Templating of Nanoparticles: A Composite Approaching Capacitance Limits in Graphene. *J. Phys. Chem. C* **2012**, *116*, 12124–12130.
32. Scott, C. L.; Pumera, M. Nanogold Spacing of Stacked Graphene Nanofibers for Supercapacitors. *Electroanalysis* **2011**, *23*, 858–861.
33. Grden, M.; Kotowski, J.; Czerwinski, A. The Study of Electrochemical Palladium Behavior Using the Quartz Crystal Microbalance. *J. Solid State Electrochem.* **2000**, *4*, 273–278.
34. Grden, M.; Czerwinski, A. EQCM Studies on Pd-Ni Alloy Oxidation in Basic Solution. *J. Solid State Electrochem.* **2008**, *12*, 375–385.
35. Liang, Z. X.; Zhao, T. S.; Xu, J. B.; Zhu, L. D. Mechanism Study of the Ethanol Oxidation Reaction on Palladium in Alkaline Media. *Electrochim. Acta* **2009**, *54*, 2203–2208.
36. Prabhuram, J.; Manoharan, R.; Vasan, H. N. Effects of incorporation of Cu and Ag in Pd on Electrochemical Oxidation of Methanol in Alkaline Solution. *J. Appl. Electrochem.* **1998**, *28*, 935–941.